PROCEEDINGS A

rspa.royalsocietypublishing.org

Research

Cite this article: Ali SZ, Dey S. 2016 Mechanics of advection of suspended particles in turbulent flow. *Proc. R. Soc. A* **472**: 20160749. http://dx.doi.org/10.1098/rspa.2016.0749

Received: 3 October 2016
Accepted: 27 October 2016

Subject Areas:
fluid mechanics, applied mathematics

Keywords:
turbulent flow, particle suspension, two-phase flow

Author for correspondence:
Sk Zeeshan Ali
e-mail: skzeeshanali@iitkgp.ac.in

Mechanics of advection of suspended particles in turbulent flow

Sk Zeeshan Ali and Subhasish Dey

Department of Civil Engineering, Indian Institute of Technology Kharagpur, West Bengal, India

SZA, 0000-0003-0763-7437

In this paper, we explore the mechanics and the turbulent structure of two-phase (fluid–solid particle) flow system, for the first time, by considering the dynamic equilibrium coupled with suspended solid particle concentration, fluid flow and energetics of the two-phase flow system. The continuity, momentum and turbulent kinetic energy (TKE) equations of the fluid and the solid phases are treated separately to derive a generalized relationship of the two-phase flow system aided by suitable closure relationships. The results obtained from the numerical solution of resulting equations show that the particle concentration and the TKE diminish with an increase in the Rouse number, while the horizontal velocity component increases. On the other hand, the TKE flux, diffusion and production rates increase with an increase in the Rouse number, while the TKE dissipation rate decreases. In the vicinity of the reference level (that is, the hypothetical level from which the particles come in suspension), the Kolmogorov number increases with an increase in the Rouse number. However, as the vertical distance increases, this behaviour becomes reverse. A close observation of the turbulent length scales reveals that the Prandtl's mixing length decreases with an increase in the Rouse number, but the Taylor microscale and the Kolmogorov length scale increase.

1. Introduction

When fluid flows over a loose boundary, the surface particles composing the boundary are subject to fluid-induced shear stress. As a consequence, particles are transported forming different layers according to their modes of transport. With an increase in boundary shear stress in excess of the threshold boundary shear stress

THE ROYAL SOCIETY PUBLISHING

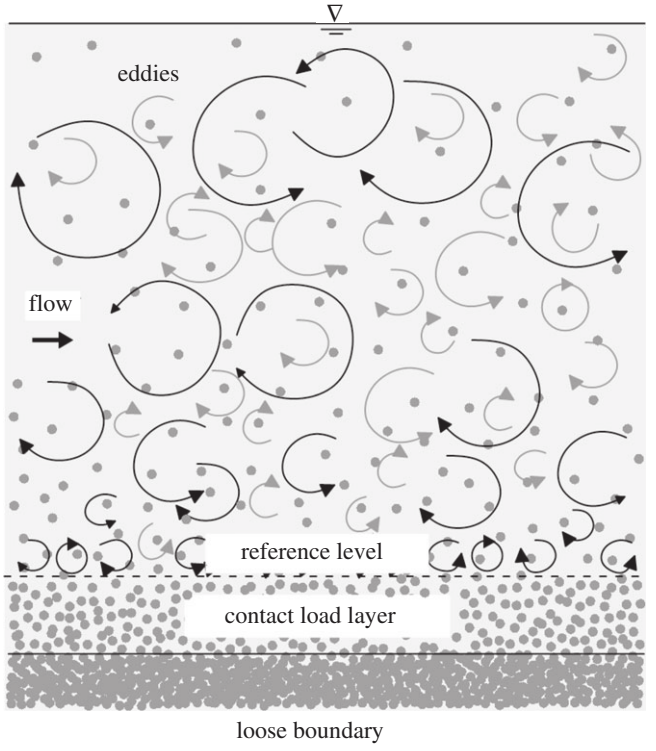

Figure 1. Conceptual description of suspended particles in turbulent free-surface flow. Density of dots signifies the concentration of particles. Reference level is shown by the broken line.

for the initiation of particle motion, the transport of particles takes place within a thin layer, known as *contact load layer*, in the form of rolling, sliding and saltating (a series of short jumps) modes. On the other hand, particles beneath the contact load layer remain immobile. With a further increase in boundary shear stress, the production of turbulence in the vicinity of the boundary acts to lift up the finer particles out of the contact load layer, maintaining them to transport in a suspension mode. A conceptual representation of suspended particles in turbulent free-surface flow is shown in figure 1, where the circular arrows represent the turbulent eddies. The tendency of a particle to settle down owing to the settling velocity is balanced by the turbulent diffusion to maintain the dynamic equilibrium. In figure 1, the density of dots signifies the particle concentration. The transport of suspended particles takes place convectively when a turbulent eddy carrying the suspended particles in its core is primarily transported by the vertical velocity fluctuations to a region of lower particle concentration and then mixes up with the ambient fluid. The determination of suspended particle concentration is usually done relative to a *reference concentration* that exists at a *reference level*. The reference level is defined as a hypothetical level of the extremity of the contact load layer in the close proximity of the loose boundary from which the solid particles come in suspension (figure 1 and table 1).

The conceptual framework of the *Fickian diffusion* [1] aided by the turbulent diffusion was widely applied to study the dynamics of suspended particles in a flowing fluid. Rouse [2] pioneered the analytical solution for the vertical profile of suspended particle concentration by means of Fickian diffusion in conjunction with the Kármán–Prandtl logarithmic velocity law. The limitation of the Rouse equation is that it predicts a vanishing particle concentration at the free surface, although the measurements evidenced a finite concentration there. The reason for the discrepancy is attributed to the assumption of the linear law of turbulent shear stress together with the logarithmic law (log-law) of velocity. Importantly, the log-law of velocity is

Table 1. Nomenclature.

a	reference level
c	instantaneous particle concentration
$\bar{c}_a$	time-averaged reference concentration
c^+	$\bar{c}/\bar{c}_a$
d	diameter of particles
E	instantaneous kinetic energy per unit volume in the two-phase flow system
E_{D}	$\varepsilon h/u_*^3$
E_{K}	time-averaged kinetic energy per unit volume resulting from mean flow
E_{T}	time-averaged TKE per unit volume resulting from velocity fluctuations
F_{kw}	f_{kw}/u_*^3
f_i	component of interaction force between fluid and particle along x_i
f_{kw}	TKE flux
G	$u_*^2/(\Delta g h)$
g_i	component of gravity force along x_i
h	flow depth
J	$u_* h/\upsilon$
Ko	Kolmogorov number
k	TKE transmitted to unit mass in the two-phase flow system
k^+	k/u_*^2
L	turbulent length scale
l	Prandtl's mixing length
l^+	l/h
p	instantaneous hydrodynamic pressure of disperse system
Q	TKE dissipation per unit volume in the two-phase flow system
Sc	turbulent Schmidt number
s_{ij}	$\partial v_i/\partial x_j + \partial v_j/\partial x_i$
T_D	$t_{\mathrm{D}} h/u_*^3$
t_D	TKE diffusion rate
T_{P}	$t_{\mathrm{P}} h/u_*^3$
t_{P}	TKE production rate
t	time
u_i	instantaneous velocity components along x_i
u_*	friction velocity
u^+	$\bar{u}/u_*$
$\bar{u}$	time-averaged horizontal flow velocity
$\tilde{u}_{\mathrm{rms}}$	$(2k^+/3)^{1/2}$
v_i	flow velocity along i of mass centre of disperse system per unit volume
x	horizontal direction

(*Continued*.)

Table 1. (*Continued*.)

y	lateral direction
Z	Rouse number [$=\omega_s \mathrm{Sc}/(\kappa u_*)$]
z	vertical direction
z^+	z/h
Δ	submerged relative density of particles [$=(\rho_\mathrm{p}-\rho_\mathrm{f})/\rho_\mathrm{f}$]
Π_{ij}	convective momentum flow density
Ω_{ij}	$\tau_{ij}^{(1)}+\tau_{ij}^{(2)}$
Ξ_j	component of current density vector of TKE along x_j resulting from molecular mixing
α_s	instantaneous hydrodynamic pressure shared by fluid phase
δ_{ij}	Kronecker delta function
ϵ	TKE dissipation rate
η	Kolmogorov length scale
η^+	η/h
κ	von Kármán constant
λ	Taylor microscale
λ^+	λ/h
υ	coefficient of kinematic viscosity of fluid
ρ_f	mass density of fluid
ρ_m	mass density of two-phase flow system
ρ_p	mass density of particles
$\tilde{\tau}$	τ/u_*^2
$\tau_{ji}^{(1)}$	component j, i of viscous stress tensor of fluid
$\tau_{ji}^{(2)}$	component j, i of stress tensor due to interaction between particles
τ	Reynolds shear stress (relative to mass density of fluid)
ω	settling velocity of particles
ω_s	settling velocity of particles in a pure quiescent fluid

based on the assumption of a constant shear stress within the wall-shear layer. After Rouse [2], several attempts were made in order to provide an improved version of the vertical distribution of suspended particle concentration. A comprehensive survey on this topic was presented by Dey [3]. Remarkably, Hunt [4] analysed the particle suspension dynamics by treating the fluid phase and the solid phase separately and then coupled both the phases by decomposing the vertical velocity of the particle into the vertical flow velocity and the particle settling velocity in a quiescent fluid.

In addition to the diffusion concept, the gravitational theory pioneered by Velikanov [5,6] provides an enhanced understanding towards the vertical profile of suspended particles arising from the principle of conservation of energy. In the gravitational theory, the fluid phase acts as the active dispersive component to perform work in carrying the particles in suspension. By contrast, the solid phase acts as the passive component because the particles consume the energetics of the system in order to remain in suspension.

Several experimental studies, based on the determinations of mean concentration and velocity [7–10] and turbulence characteristics of the two-phase flow system [11–13], were

reported. Lagrangian and Eulerian particle tracking methods were applied in particle-laden flows to study the behaviour of two-phase flow [14–19]. The transport of massive particles in fluid was modelled by Hsu *et al*. [20]. On the other hand, the rheology of solid particle suspension was studied by Mueller *et al*. [21]. Recently, Cantero-Chinchilla *et al*. [22] developed a power law theory to determine the concentration profile of particle-laden flow. However, they did not consider the energetics of the two-phase flow system.

The major drawback of the diffusion theory in modelling the dynamics of suspended particles is due to the questionable assumption, which states that the dynamics of fluid flow remains unaffected by the presence of suspended particles. Further, with regard to the gravitational theory, the primary shortcoming is that the reduction in pulsation energy resulting from the work done to keep the particles in suspension is ignored.

Here, we present the mechanics and the turbulent structure of the two-phase flow system by taking into account the dynamic coupling of suspended particle concentration, flow velocity and energetics of the two-phase flow system. A generalized formulation of the two-phase flow system is derived by treating separately the equations of motion of fluid and solid phases. The resulting equations are numerically solved applying closure relationships. The profiles of suspended particle concentration, horizontal velocity component and turbulent kinetic energy (TKE) are obtained. Further, the profiles of TKE flux, diffusion rate, production rate, dissipation rate, the Kolmogorov number and turbulent length scales are determined. The variations of these profiles with the Rouse number are depicted.

2. Theoretical analysis

We consider a two-phase flow system, where both the relative volume and the particle size are small. The instantaneous fluid acceleration can be fairly neglected in comparison with the gravitational acceleration. We further assume that the molecular diffusion of suspended particles is vanishingly small and therefore neglected. Under such assumptions, the equation of motion of fluid phase is [23]

$$\frac{\partial}{\partial t}[\rho_{\mathrm{f}}(1-c)u_{\mathrm{f}i}] + \frac{\partial}{\partial x_j}[\rho_{\mathrm{f}}(1-c)u_{\mathrm{f}i}u_{\mathrm{f}j}] = -\frac{\partial}{\partial x_i}(\alpha_{\mathrm{s}}p) + \frac{\partial \tau_{ji}^{(1)}}{\partial x_i} + \rho_{\mathrm{f}}(1-c)g_i - f_i, \tag{2.1}$$

and the equation of motion of solid phase is [23]

$$\frac{\partial}{\partial t}(\rho_{\mathrm{p}}cu_{\mathrm{p}i}) + \frac{\partial}{\partial x_j}(\rho_{\mathrm{p}}cu_{\mathrm{p}i}u_{\mathrm{p}j}) = -\frac{\partial}{\partial x_i}[(1-\alpha_{\mathrm{s}})p] + \frac{\partial \tau_{ji}^{(2)}}{\partial x_i} + \rho_{\mathrm{p}}cg_i + f_i. \tag{2.2}$$

In equations (2.1) and (2.2), subscripts 'f' and 'p' refer to the quantities related to fluid and particle, respectively, t is the time, ρ is the mass density, c is the instantaneous suspended particle concentration, u_i and u_j are the instantaneous velocity components along x_i and x_j, respectively, $i=1$, 2 and 3 denote the x (horizontal), y (lateral) and z (vertical) directions, respectively, p is the instantaneous hydrodynamic pressure of the disperse system, α_{s} is the instantaneous hydrodynamic pressure shared by the fluid phase, $\tau_{ji}^{(1)}$ is the component j, i of the viscous stress tensor of fluid, g_i is the component of gravity force along x_i, f_i is the component of the interaction force between fluid and particle along x_i and $\tau_{ji}^{(2)}$ is the component j, i of the stress tensor due to interaction between the particles.

The mass density ρ_{m} of the two-phase flow system is defined by

$$\rho_{\mathrm{m}} = \rho_{\mathrm{f}}(1-c) + \rho_{\mathrm{p}}c. \tag{2.3}$$

The flow velocity along i of the mass centre of the disperse system per unit volume is

$$v_i = \frac{\rho_{\mathrm{f}}(1-c)u_{\mathrm{f}i} + \rho_{\mathrm{p}}cu_{\mathrm{p}i}}{\rho_{\mathrm{m}}}. \tag{2.4}$$

The equation of motion of the disperse system, after adding equations (2.1) and (2.2), yields

$$\frac{\partial}{\partial t}(\rho_{\mathrm{m}} v_i) + \frac{\partial \Pi_{ij}}{\partial x_j} = -\frac{\partial p}{\partial x_i} + \frac{\partial \Omega_{ji}}{\partial x_i} + \rho_{\mathrm{m}} g_i. \tag{2.5}$$

In equation (2.5), Π_{ij} is the convective momentum flow density defined by

$$\Pi_{ij} = \rho_{\mathrm{f}}(1-c)u_{\mathrm{f}i}u_{\mathrm{f}j} + \rho_{\mathrm{p}} c u_{\mathrm{p}i}u_{\mathrm{p}j}. \tag{2.6}$$

The conductive counterpart appearing in equation (2.5) is $\Omega_{ij} = \tau_{ij}^{(1)} + \tau_{ij}^{(2)}$. When the particle concentration is very small, the tensor $\tau_{ji}^{(2)}$ becomes much smaller than the tensor $\tau_{ji}^{(1)}$.

The continuity equations for the fluid phase and the solid phase are, respectively,

$$\frac{\partial}{\partial t}[\rho_{\mathrm{f}}(1-c)] + \frac{\partial}{\partial x_j}[\rho_{\mathrm{f}}(1-c)u_{\mathrm{f}j}] = 0 \tag{2.7}$$

and

$$\frac{\partial}{\partial t}(\rho_{\mathrm{p}} c) + \frac{\partial}{\partial x_j}(\rho_{\mathrm{p}} c u_{\mathrm{p}j}) = 0. \tag{2.8}$$

The continuity equation of the two-phase flow system, after combining equations (2.7) and (2.8), is therefore

$$\frac{\partial \rho_{\mathrm{m}}}{\partial t} + \frac{\partial}{\partial x_j}(\rho_{\mathrm{m}} v_j) = 0. \tag{2.9}$$

Moreover, from equations (2.7) and (2.8), we obtain

$$\frac{\partial}{\partial x_j}[(1-c)u_{\mathrm{f}j} + c u_{\mathrm{p}j}] = 0. \tag{2.10}$$

As the particle concentration is small and the fluid acceleration is considered relatively smaller in comparison with the gravitational acceleration, we can fairly approximate that the instantaneous horizontal velocity components of fluid and particle coincide. By contrast, the instantaneous vertical velocity components of fluid and particle differ by the settling velocity ω of particles. Specifically, the ω is a function of the particle diameter d [3]. Therefore, it yields

$$u_{\mathrm{f}i} - u_{\mathrm{p}i} = \delta_{i3}\omega, \tag{2.11}$$

where δ_{ij} is the Kronecker delta function defined by $\delta_{ij}(i \neq j) = 0$ and $\delta_{ij}(i = j) = 1$.

Using equations (2.10) and (2.11), partial differentiation of equation (2.4) yields

$$\frac{\partial v_j}{\partial x_j} = -(\rho_{\mathrm{p}} - \rho_{\mathrm{f}})\frac{\partial}{\partial z}\left[\frac{\omega c(1-c)}{\rho_{\mathrm{m}}}\right]. \tag{2.12}$$

With allowance to equation (2.12), equation (2.9) reduces to

$$\frac{\partial \rho_{\mathrm{m}}}{\partial t} + v_j \frac{\partial \rho_{\mathrm{m}}}{\partial x_j} = \rho_{\mathrm{m}}(\rho_{\mathrm{p}} - \rho_{\mathrm{f}})\frac{\partial}{\partial z}\left[\frac{\omega c(1-c)}{\rho_{\mathrm{m}}}\right]. \tag{2.13}$$

Furthermore, differentiating partially equation (2.6) and using equations (2.4) and (2.11), we obtain

$$\frac{\partial \Pi_{ij}}{\partial x_j} = \frac{\partial}{\partial x_j}(\rho_{\mathrm{m}} v_i v_j) + \rho_{\mathrm{f}}\rho_{\mathrm{p}}\frac{\partial}{\partial z}\left[\frac{\omega^2 c(1-c)}{\rho_{\mathrm{m}}}\right]\delta_{i3}. \tag{2.14}$$

Thus, equation (2.5) becomes

$$\frac{\partial}{\partial t}(\rho_{\mathrm{m}} v_i) + \frac{\partial}{\partial x_j}(\rho_{\mathrm{m}} v_i v_j) = \rho_{\mathrm{m}} g_i - \frac{\partial p}{\partial x_i} + \frac{\partial \Omega_{ji}}{\partial x_i} - \rho_{\mathrm{f}}\rho_{\mathrm{p}}\frac{\partial}{\partial z}\left[\frac{\omega^2 c(1-c)}{\rho_{\mathrm{m}}}\right]\delta_{i3}. \tag{2.15}$$

Introducing the submerged relative density of particles Δ $[=(\rho_p-\rho_f)/\rho_f]$ and noting that $\rho_m=\rho_f(1+\Delta c)$, equations (2.12), (2.13) and (2.15) reduce to

$$\frac{\partial v_j}{\partial x_j}=-\Delta\frac{\partial}{\partial z}\left[\frac{\omega c(1-c)}{1+\Delta c}\right], \tag{2.16}$$

$$\frac{\partial c}{\partial t}+v_j\frac{\partial c}{\partial x_j}=(1+\Delta c)\frac{\partial}{\partial z}\left[\frac{\omega c(1-c)}{1+\Delta c}\right] \tag{2.17}$$

and

$$\frac{\partial}{\partial t}[(1+\Delta c)v_i]+\frac{\partial}{\partial x_j}[(1+\Delta c)v_iv_j]=(1+\Delta c)g_i-\frac{1}{\rho_f}\frac{\partial p}{\partial x_i}+\frac{1}{\rho_f}\frac{\partial \Omega_{ji}}{\partial x_i}-(1+\Delta)\frac{\partial}{\partial z}\left[\frac{\omega^2c(1-c)}{1+\Delta c}\right]\delta_{i3}. \tag{2.18}$$

Applying the Reynolds decomposition, we split the instantaneous velocity and particle concentration as $v_i=\bar{v}_i+v_i'$ and $c=\bar{c}+c'$, where over-bar denotes the time-averaged quantities and prime denotes the fluctuations. Here, the time-averaged velocity components $\bar{v}_i(i=1,2,3)$ are $(\bar{u},\bar{v},\bar{w})$, respectively. Thus, in time-averaged form, equations (2.16)–(2.18) are

$$\frac{\partial \bar{v}_j}{\partial x_j}=-\Delta\frac{\partial}{\partial z}\left[\frac{\omega\bar{c}(1-\bar{c})}{1+\Delta\bar{c}}\right], \tag{2.19}$$

$$\frac{\partial\bar{c}}{\partial t}+\bar{v}_j\frac{\partial\bar{c}}{\partial x_j}=-\frac{\partial}{\partial x_j}(\overline{c'v_j'})+(1+\Delta\bar{c})\frac{\partial}{\partial z}\left[\frac{\omega\bar{c}(1-\bar{c})}{1+\Delta\bar{c}}\right] \tag{2.20}$$

and

$$\frac{\partial}{\partial t}[\overline{(1+\Delta c)v_i}]+\frac{\partial}{\partial x_j}[\overline{(1+\Delta c)v_iv_j}]=(1+\Delta\bar{c})g_i-\frac{1}{\rho_f}\frac{\partial\bar{p}}{\partial x_i}+\frac{1}{\rho_f}\frac{\partial\bar{\Omega}_{ji}}{\partial x_i}-(1+\Delta)\frac{\partial}{\partial z}\left[\frac{\omega^2\bar{c}(1-\bar{c})}{1+\Delta\bar{c}}\right]\delta_{i3}. \tag{2.21}$$

Equations (2.19)–(2.21) represent the generalized formulation of the fluid–particle system. Now, we intend to introduce the energetics of the two-phase flow system by balancing the energy of the system.

The instantaneous kinetic energy per unit volume in the two-phase flow system is

$$E=\tfrac{1}{2}\rho_m v_i^2. \tag{2.22}$$

The time-averaged form of equation (2.22) is thus

$$\bar{E}=\underbrace{\tfrac{1}{2}\bar{\rho}_m\bar{v}_i^2}_{E_K}+\underbrace{\overline{\rho_m'v_j'}\bar{v}_j+\tfrac{1}{2}\bar{\rho}_m\overline{v_i'^2}}_{E_T}. \tag{2.23}$$

In equation (2.23), the E_K signifies the time-averaged kinetic energy per unit volume in the two-phase flow system resulting from the mean flow, while the E_T represents the time-averaged TKE per unit volume in the two-phase flow system resulting from the fluctuations. Hence, the energy balance equation becomes

$$\frac{d\bar{E}}{dt}=\frac{dE_K}{dt}+\frac{dE_T}{dt}. \tag{2.24}$$

Using the mathematical operation $d(\cdot)/dt=\partial(\cdot)/\partial t+v_j\partial(\cdot)/\partial x_j$ and neglecting the smaller order terms, the energy balance of the two-phase flow system is obtained as

$$\frac{\partial E_T}{\partial t}+\bar{v}_j\frac{\partial E_T}{\partial x_j}=-\overline{\rho_m'w'}g-\overline{\frac{\partial p'}{\partial x_j}v_j'}+\frac{\partial\Xi_j}{\partial x_j}-Q-\frac{\partial}{\partial x_j}\left(\frac{1}{2}\rho_f\overline{v_i'^2v_j'}\right)-\frac{1}{2}\rho_f\overline{v_i'v_j'}\bar{s}_{ij}, \tag{2.25}$$

where $\Xi_j=\overline{v_i\Omega_{ji}'}$ defining the component of the current density vector of the TKE along x_j, resulting from molecular mixing, $Q=0.5\overline{\Omega_{ij}'s_{ij}'}$ describing the TKE dissipation per unit volume in the two-phase flow system and $s_{ij}=\partial v_i/\partial x_j+\partial v_j/\partial x_i$. The terms appearing in the right-hand side

of equation (2.25) can be interpreted as follows: the first term signifies the loss in TKE in lifting the particles. The second term describing the gain in TKE resulting from the work done owing to pressure fluctuations is vanishingly small and therefore neglected. The third term denotes the gain in TKE resulting from molecular mixing. The fourth term designates the TKE dissipation. The fifth term represents the gain in TKE owing to turbulent mixing and the last term expresses the gain in TKE resulting from the energy of time-averaged flow.

Under two-dimensional steady homogeneous turbulent flow, equations (2.19)–(2.21) and (2.25) reduce to

$$\frac{\mathrm{d}\bar{w}}{\mathrm{d}z} = -\Delta \frac{\mathrm{d}}{\mathrm{d}z}\left[\frac{\omega\bar{c}(1-\bar{c})}{1+\Delta\bar{c}}\right], \tag{2.26}$$

$$\bar{w}\frac{\mathrm{d}\bar{c}}{\mathrm{d}z} = -\frac{\mathrm{d}}{\mathrm{d}z}(\overline{c'w'}) + (1+\Delta\bar{c})\frac{\mathrm{d}}{\mathrm{d}z}\left[\frac{\omega\bar{c}(1-\bar{c})}{1+\Delta\bar{c}}\right], \tag{2.27}$$

$$\frac{\mathrm{d}}{\mathrm{d}z}[(1+\Delta\bar{c})(\bar{u}\bar{w}+\overline{u'w'}) + \Delta\bar{u}\overline{c'w'}] = \frac{u_*^2}{h}(1+\Delta\bar{c}) \tag{2.28}$$

and

$$\bar{w}\frac{\mathrm{d}E_\mathrm{T}}{\mathrm{d}z} + \Delta\rho_\mathrm{f}\overline{c'w'}g + Q + \frac{\mathrm{d}}{\mathrm{d}z}\left(\frac{1}{2}\rho_\mathrm{f}\overline{v_i'^2 w'}\right) + \rho_\mathrm{f}\overline{u'w'}\frac{\mathrm{d}\bar{u}}{\mathrm{d}z} + \frac{1}{2}\rho_\mathrm{f}\overline{w'^2}\frac{\mathrm{d}\bar{w}}{\mathrm{d}z} = 0, \tag{2.29}$$

where h is the flow depth and u_* is the friction velocity.

Integrating equation (2.26) results in

$$\bar{w} = -\Delta\left[\frac{\omega\bar{c}(1-\bar{c})}{1+\Delta\bar{c}}\right], \tag{2.30}$$

where the integration constant is assumed to be zero, as the vertical velocity vanishes at the free surface.

Inserting equation (2.30) into equation (2.27) and performing the integration yield

$$\overline{c'w'} = \omega\bar{c}(1-\bar{c}). \tag{2.31}$$

Further, integration of equation (2.28) with the boundary condition $-\overline{u'w'}|_{z=0} = u_*^2$ and using equations (2.30) and (2.31) yield

$$\tilde{\tau} = 1 - z^+, \tag{2.32}$$

where $\tilde{\tau}$ is τ/u_*^2, τ is the Reynolds shear stress (relative to mass density of fluid ρ_f) given by $-\overline{u'w'}$ and z^+ is z/h. Equation (2.32) reveals that the Reynolds shear stress profile, even in a two-phase flow system, displays a linear variation with the vertical distance when the velocity fluctuations of fluid flow are replaced by the velocity fluctuations in the two-phase flow system. To check the validity of equation (2.32), we consider the experimental data of Lyn [9] (runs 1957EQ and 1965EQ) and Cellino & Graf [11] (runs SLF3 and SAT), as depicted in figure 2. A brief summary of the experimental conditions is furnished in table 2. Figure 2 shows that the computed $\tilde{\tau}(z^+)$ profiles have an excellent agreement with the experimental data. However, for $z^+ < 0.18$, the experimental data of Cellino & Graf [11] depart from the linear relationship (equation (2.32)). This is attributed to the fact that for $z^+ < 0.18$, the Reynolds shear stress profile exhibits a considerable damping owing to the reduced velocity fluctuations in the vicinity of the boundary. In fact, equation (2.32) represents the total shear stress profile (summation of Reynolds shear stress and viscous shear stress). As the viscous shear stress is practically negligible except within the thin viscous sub-layer, the Reynolds shear stress composes the total shear stress. Therefore, equation (2.32) is legitimate above the viscous sub-layer.

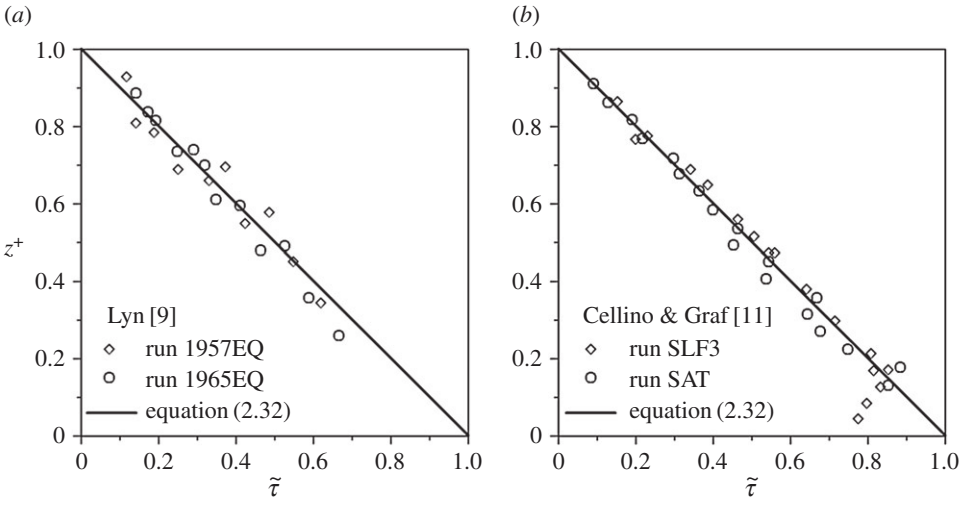

Figure 2. Computed $\tilde{\tau}$ profiles compared with the experimental data of Lyn [9] and Cellino & Graf [11].

Table 2. Brief summary of experimental conditions.

author	run	h (mm)	d (mm)	u_* (m s^{-1})	Z
Montes [7]	20	73	0.3899	0.06917	2
	24	77	0.3899	0.06112	2.3
Coleman [8]	22	170	0.21	0.041	0.75
	33	174	0.42	0.041	0.8
Lyn [9]	1957EQ	57.2	0.19	0.0395	1.4
	1965EQ	65.1	0.19	0.0375	1.5
	1957ST2A	58.4	0.19	0.0425	1.5
	1957ST2B	57.7	0.19	0.0431	1.2
Cellino & Graf [11]	SLF3	120	0.135	0.045	0.674
	SAT	120	0.135	0.045	0.667

Because equations (2.26)–(2.29) do not form a closed system, we adopt the following closure relationships:

$$\overline{v_i' v_j'} = \frac{2}{3} k \delta_{ij} - \sigma_1 s_{ij}, \tag{2.33}$$

$$\frac{1}{2} \sum_{j=1}^{3} \sum_{i=1}^{3} \overline{v_i'^2 v_j'} = -\sigma_2 \sum_{j=1}^{3} \frac{\partial k}{\partial x_j} \tag{2.34}$$

and

$$\sum_{j=1}^{3} \overline{c' v_j'} = -\sigma_3 \sum_{j=1}^{3} \frac{\partial \bar{c}}{\partial x_j}, \tag{2.35}$$

where k represents the TKE transmitted to unit mass in the two-phase flow system and σ_1, σ_2 and σ_3 are the scalar coefficients. Introducing the turbulent length scale L, we can write $\sigma_1 = \sigma_2 = Lk^{1/2}$ and $\sigma_3 = Lk^{1/2}/\mathrm{Sc}$ [24], where Sc is the turbulent Schmidt number, a phenomenological constant, which is considered here as unity, for simplicity. The L can be expressed as $L = \kappa \gamma z$ [25], where κ

is the von Kármán constant (=0.41) and γ is the universal constant (=0.5) [25]. Furthermore, the Q in equation (2.29) is expressed as $Q = \rho_f \gamma^4 k^{3/2}/L$ [24,25].

Measurements evidenced that in fluid with suspended particles, the flow around the neighbouring settling particles induces a larger drag in comparison with that in a pure fluid (without particles), known as *hindered settling effect*. This effect yields a settling velocity in a two-phase flow system (particle-laden fluid) to reduce from that in a pure fluid. Thus, we write $\omega = \omega_s(1-\bar{c})^n$ [26], where ω_s is the settling velocity in a pure quiescent fluid and n is an exponent. Under such consideration and using the closure relationships (equations (2.33)–(2.35)) in conjunction with equations (2.30)–(2.32), equations (2.26)–(2.29) reduce to the following three equations:

$$\frac{\mathrm{d}\bar{c}}{\mathrm{d}z^+} = -\frac{Z\bar{c}(1-\bar{c})^{1+n}}{\gamma z^+ k^{+1/2}}, \tag{2.36}$$

$$\frac{\mathrm{d}u^+}{\mathrm{d}z^+} = \frac{1-z^+}{\kappa\gamma z^+ k^{+1/2}}, \tag{2.37}$$

and

$$k^{+1/2}z^+\frac{\mathrm{d}^2k^+}{\mathrm{d}z^{+2}} + \left(\frac{z^+}{2k^{+1/2}}\cdot\frac{\mathrm{d}k^+}{\mathrm{d}z^+} + k^{+1/2}\right)\frac{\mathrm{d}k^+}{\mathrm{d}z^+} = \frac{Z}{G\gamma}\bar{c}(1-\bar{c})^{1+n} + \frac{\gamma^2}{\kappa^2}\cdot\frac{k^{+3/2}}{z^+} - \frac{1}{(\kappa\gamma)^2}\cdot\frac{(1-z^+)^2}{k^{+1/2}z^+}, \tag{2.38}$$

where Z is the Rouse number $[=\omega_s \mathrm{Sc}/(\kappa u_*)]$, k^+ is k/u_*^2, u^+ is $\bar{u}/u_*$ and G is $u_*^2/(\Delta g h)$. Equations (2.36)–(2.38), illustrating the complete dynamics of the two-phase flow system, provide a closed form solution that can be obtained numerically subject to specified boundary conditions.

3. Numerical implementation and boundary conditions

To solve the above set of equations, we set a reference level at $z = a$, where the reference horizontal velocity, the reference concentration $\bar{c}_a$ and the reference TKE are being specified. For the numerical computations, we set the reference values as $a^+ (=a/h) = 5\times10^{-2}$, $u^+ (z^+ = a^+) = 15$, $\bar{c}_a = 10^{-3}$ and $k^+ (z^+ = a^+) = \gamma^{-2}$ [25]. These reference values may change depending on the experimental conditions. At the free surface ($z = h$), we set a vanishing flux boundary condition suggesting $\partial k/\partial z \approx 0$. To compute the theoretical curves in subsequent figures, we assume $g = 9.81\,\mathrm{m\,s^{-2}}$, $h = 0.15\,\mathrm{m}$, $u_* = 5\times10^{-2}\,\mathrm{m\,s^{-1}}$ and $\Delta = 1.65$, implying $G = 10^{-3}$. According to Richardson & Zaki [26], n varies from 4.9 to 2.3 depending on the particle Reynolds number varying from 10^{-1} to 10^3. Here, we consider $n = 4$ as an average natural integer. However, to validate the results with the experimental data, suitable boundary conditions are considered from the experimental conditions. With these considerations, equation (2.38) is first transformed to two ordinary differential equations of the first order. Then, the system of resulting equations is simultaneously solved numerically to illustrate the evolution of different key parameters and the turbulent structure of the two-phase flow system.

4. Results and discussion

Here, we present the vertical profiles of suspended particle concentration, horizontal velocity, TKE, TKE flux, TKE diffusion rate, TKE production rate, TKE dissipation rate, the Kolmogorov number and turbulent length scales. We also investigate their variations with the Rouse number. For the validation of model results, we consider the experimental data of several investigators. The experimental conditions are briefly summarized in table 2.

In figure 3, we plot the normalized concentration $c^+ (=\bar{c}/\bar{c}_a)$ as a function of normalized vertical distance z^+ for different Z (= 2, 1, 0.5 and 0.25). As a smaller value of Z indicates finer particles, c^+ for a given z^+ diminishes with an increase in Z. For finer particles, finite values of c^+ at the free surface ($z^+ = 1$) are meaningful, while for coarser particles, the c^+ at the free surface becomes

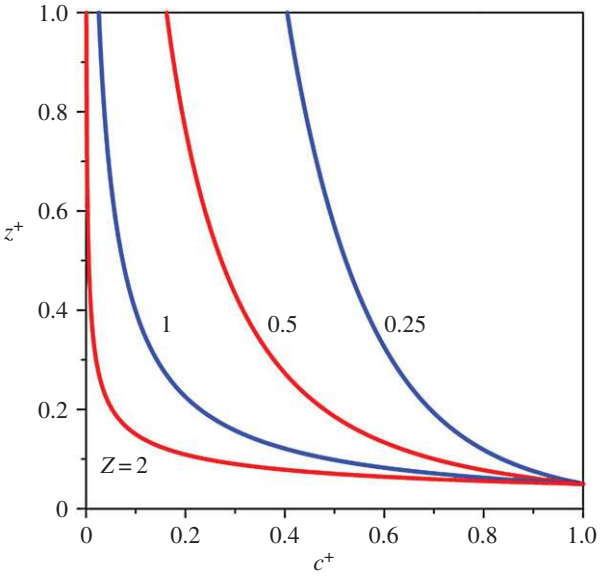

Figure 3. Computed $c^+(z^+)$ profiles for different Z (=2, 1, 0.5 and 0.25). (Online version in colour.)

vanishingly small. Interestingly, for $z^+ < 0.2$, the set of $c^+(z^+)$ curves for different Z are converging in nature.

Figure 4 shows the comparison between the computed $c^+(z^+)$ profiles and the experimental data of Montes [7] for runs 20 and 24, Coleman [8] for runs 22 and 33, and Lyn [9] for runs 1957ST2A and 1957ST2B. Overall, the computed profiles have a satisfactory agreement with the experimental data, excepting the experimental data of Lyn [9], for which the computed $c^+(z^+)$ profiles slightly overestimate the experimental data.

As the suspended particles suppress turbulence resulting from the energetics of the two-phase flow system, equation (2.37) shows that the velocity gradient increases with the suspended particle concentration. It indicates that the local strain rate of fluid element enhances in a two-phase flow system. This phenomenon corroborates with the observations of Bennett *et al*. [13]. It is worth noting that a satisfactory comparison of computed $c^+(z^+)$ profiles with the experimental data is not the sufficient condition to test the performance of an analytical model. This is attributed to the fact that the $c^+(z^+)$ and $u^+(z^+)$ profiles are mutually dependent. Therefore, a simultaneous comparison of the theoretical $c^+(z^+)$ and $u^+(z^+)$ profiles with the corresponding measurements would be more useful. For this reason, in figure 5, we show the computed $u^+(z^+)$ profiles compared with the experimental data of Montes [7], Coleman [8] and Lyn [9] for the same runs as considered in figure 4. In figure 5, the computed $u^+(z^+)$ profiles, in general, have a good agreement with the experimental data. However, the computed $u^+(z^+)$ profiles marginally depart from the experimental data of Lyn [9]. The departure of the computed $c^+(z^+)$ and $u^+(z^+)$ profiles from the experimental data is due to the presence of strong secondary currents, which can significantly change the dynamics of suspended particles by affecting the concentration and velocity profiles.

Figure 6 depicts the variation of k^+ with z^+ for different Z (= 2, 1, 0.5 and 0.25). As the suspended particles weaken the strength of the turbulent eddies to carry the particles, the resulting TKE must diminish [13]. In other words, the work done to keep the particles in suspension is to reduce the turbulence resistance in particular and therefore, the TKE reduces. Moreover, the coarser particles are to reduce the turbulence strength more than the finer ones as the local strain rate of fluid element tries to suppress the turbulence fluctuations. Hence, for a

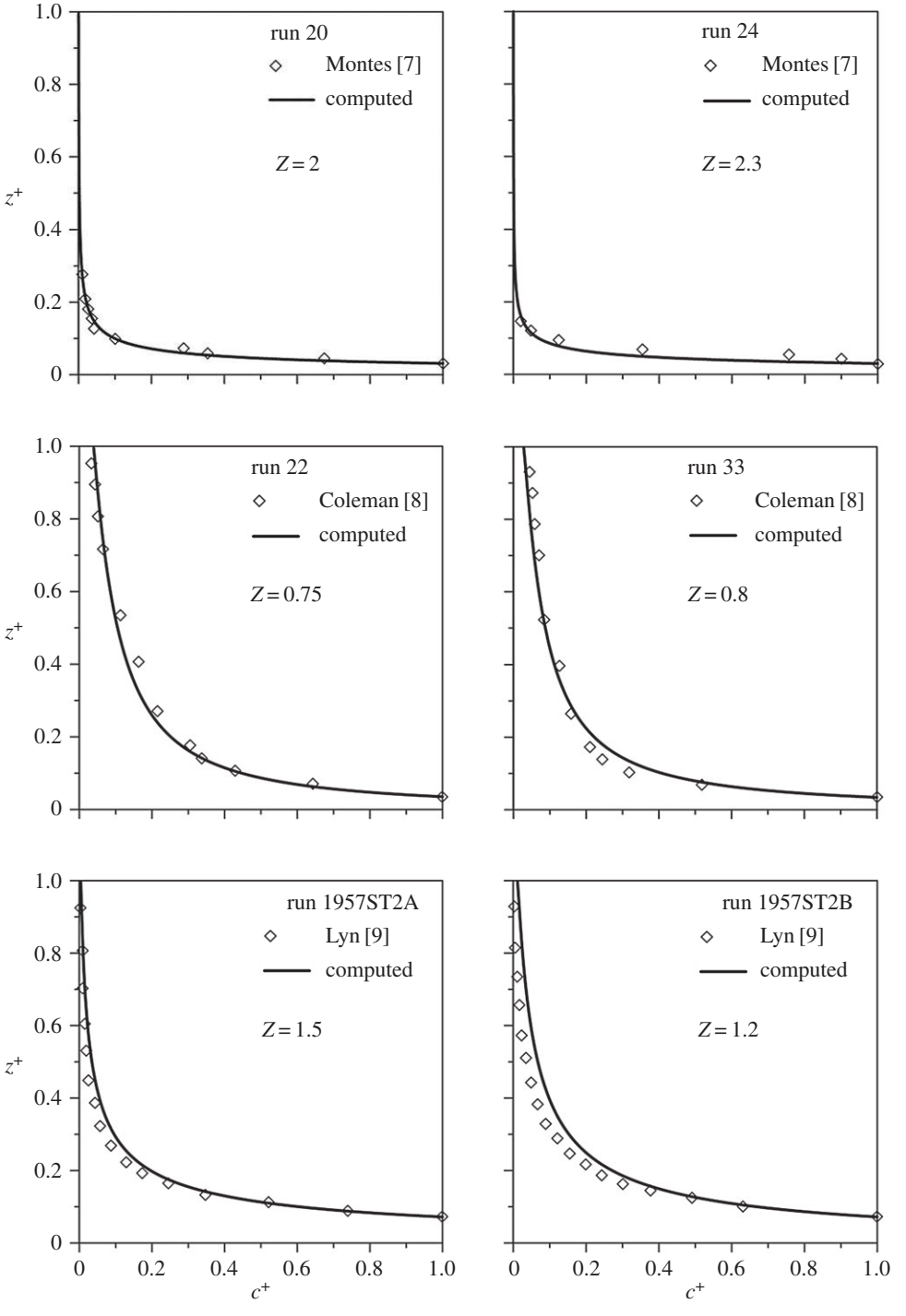

Figure 4. Computed $c^+(z^+)$ profiles compared with the experimental data of Montes [7], Coleman [8] and Lyn [9].

given z^+, the k^+ reduces with an increase in Z. On the other hand, for a given Z, the k^+ decreases with an increase in z^+ satisfying the no-flux boundary condition, that is, $\partial k^+/\partial z^+ \approx 0$ at $z^+ = 1$.

Considering isotropic turbulence, we can write the horizontal turbulence intensity as $\tilde{u}_{\mathrm{rms}}[= (\overline{u'u'})^{1/2}/u_*] = (2k^+/3)^{1/2}$. The computed $\tilde{u}_{\mathrm{rms}}(z^+)$ profiles are compared with the experimental data of Cellino & Graf [11] for runs SLF3 and SAT, as shown in figure 7. The comparison is more

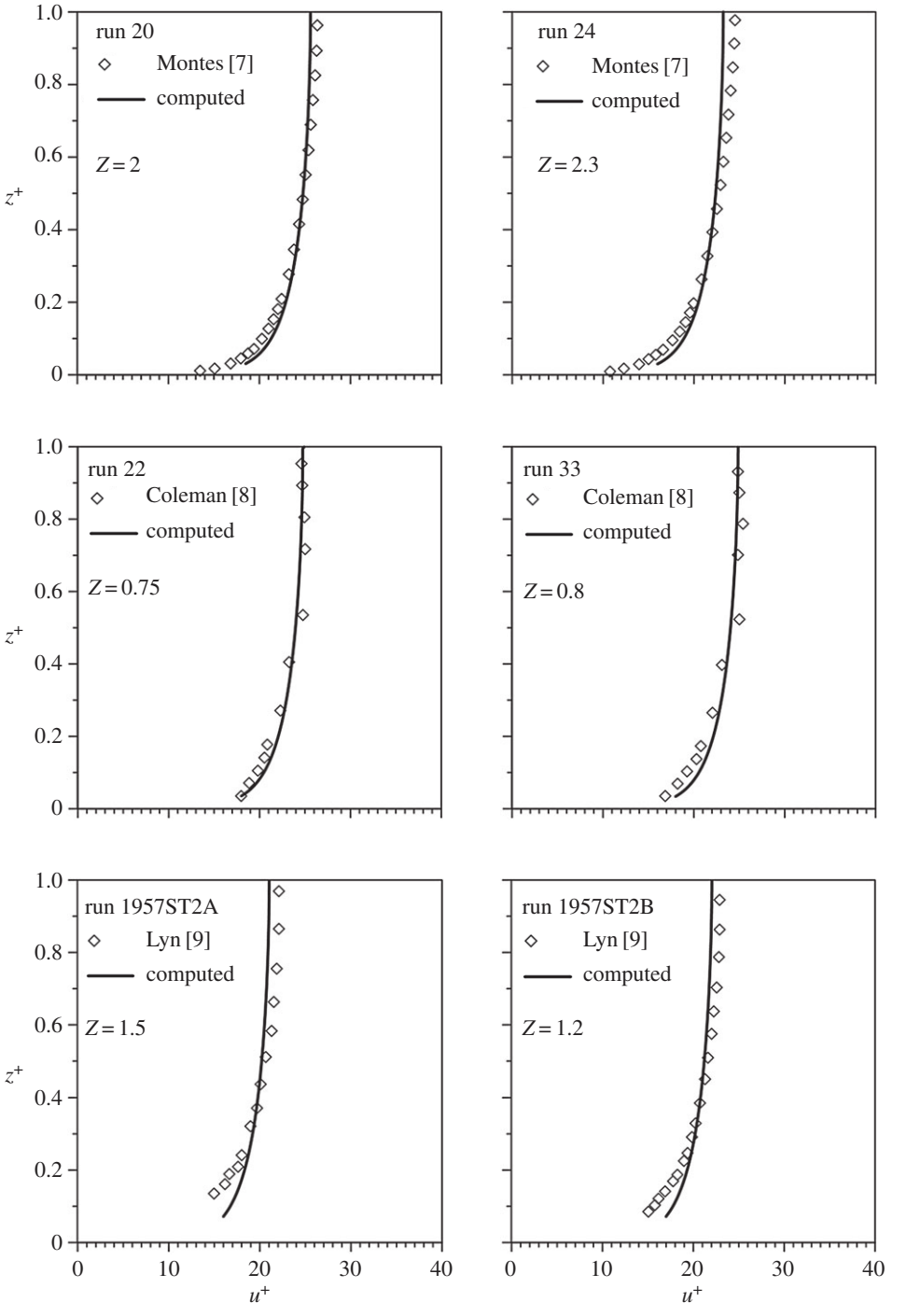

Figure 5. Computed $u^+(z^+)$ profiles compared with the experimental data of Montes [7], Coleman [8] and Lyn [9].

satisfactory for run SAT than run SLF3. A slight departure of the computed $\tilde{u}_{\mathrm{rms}}(z^+)$ profiles from the experimental data for run SLF3 is possibly due to the uncertainties associated with the measurement of instantaneous velocity close to the free surface.

The TKE flux, obtained from equation (2.34), is expressed as $f_{kw} = -Lk^{1/2}\partial k/\partial z$. Figure 8 represents the variation of normalized TKE flux $F_{kw}(=f_{kw}/u_*^3)$ with z^+ for different $Z\,(=0.25,\ 0.5,$

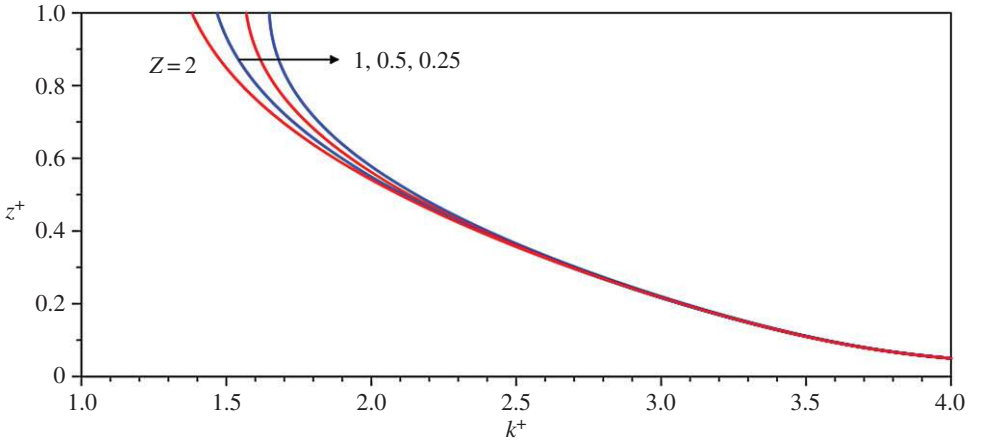

Figure 6. Computed $k^+(z^+)$ profiles for different Z (=2, 1, 0.5 and 0.25). (Online version in colour.)

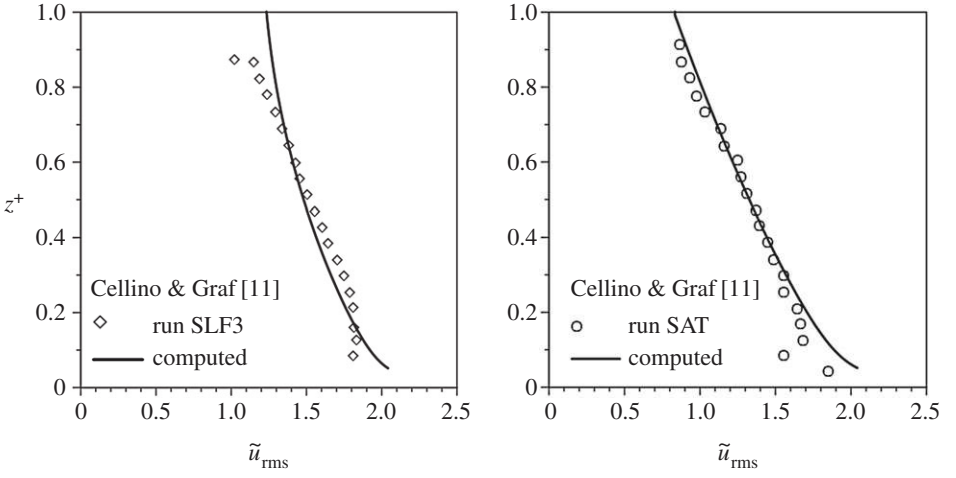

Figure 7. The computed $\tilde{u}_{\mathrm{rms}}(z^+)$ profiles compared with the experimental data of Cellino & Graf [11].

1 and 2). Because the F_{kw} is influenced by the combined action of the local TKE and its gradient, it is found that for a given Z, the $F_{kw}(z^+)$ profiles appear as inverted S-shaped curves, forming two protuberances. Figure 6 shows that for a given Z, the $\partial k^+/\partial z^+$ is essentially negative, while for a given z^+, the k^+ reduces with an increase in Z. As the decay of $\partial k^+/\partial z^+$ with z^+ is faster than that of k^+, the F_{kw} for a given z^+ increases with an increase in Z, indicating that the coarser particles are more effective to enhance the TKE flux than the finer ones.

The TKE diffusion rate is defined as $t_D = \partial f_{kw}/\partial z$. The variation of normalized TKE diffusion rate $T_D(=t_D h/u_*^3)$ with z^+ for different $Z(=0.25,\ 0.5,\ 1$ and $2)$ is illustrated in figure 9. In the vicinity of the boundary and most of the upper region, the T_D is negative, while in the intermediate region, it is positive. For a clear understanding, an enlarged frame bounded by $z^+ \in [0.9,\ 1]$ and $T_D \in [-0.8,\ -0.4]$ shows the typical variation of T_D with z^+ for different Z. It is evident that for a given z^+, T_D increases with an increase in Z. This represents that the coarser particles are to increase the TKE diffusion rate in a two-phase flow system.

Furthermore, we are interested to analyse the characteristics of TKE production rate (t_{P}) and TKE dissipation rate (ϵ) in the two-phase flow system. By definition, they are given by $t_{\mathrm{P}} = \tau(\partial\bar{u}/\partial z)$ and $\epsilon = Q/\rho_{\mathrm{f}} = \gamma^4 k^{3/2}/L$. The normalized t_{P} and ϵ are expressed as $(T_{\mathrm{P}}, E_{\mathrm{D}}) =$

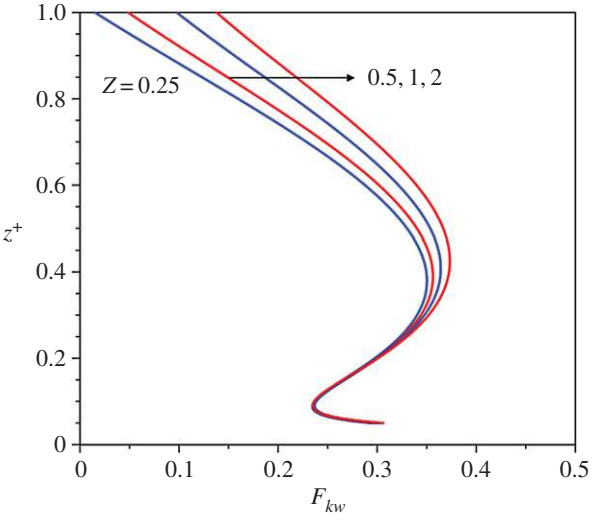

Figure 8. Computed $F_{kw}(z^+)$ profiles for different Z (= 0.25, 0.5, 1 and 2). (Online version in colour.)

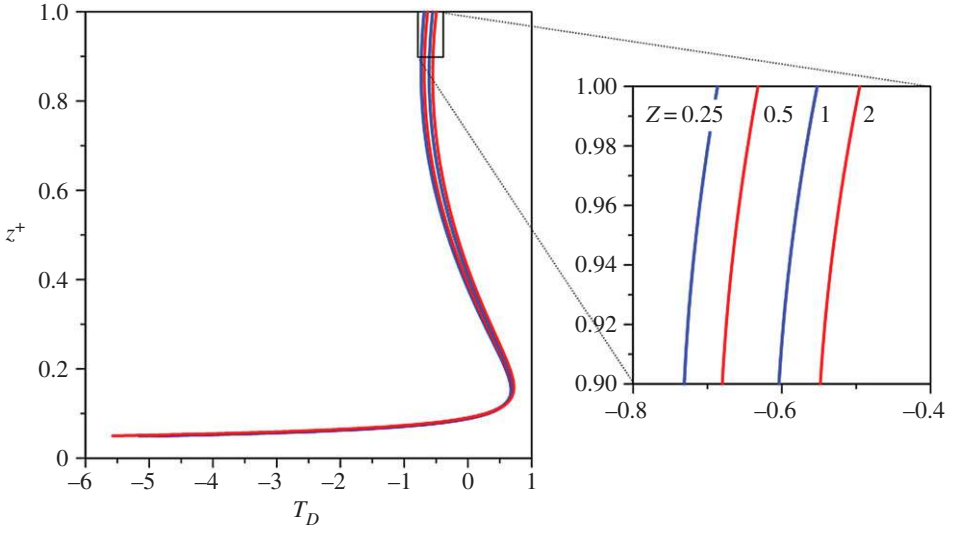

Figure 9. Computed $T_D(z^+)$ profiles for different Z (=0.25, 0.5, 1 and 2). (Online version in colour.)

$(t_P, \varepsilon) \times h/u_*^3$. The variation of T_P with z^+ for different Z (= 0.25, 0.5, 1 and 2) is presented in figure 10. The enlarged frames bounded by $z^+ \in [0.9, 1]$ and $T_P \in [0, 0.05]$ and $z^+ \in [0.94, 0.95]$ and $T_P \in [0.01, 0.016]$, respectively, help to envisage the typical variation of T_P with z^+ for different Z. Figure 10 shows that for a given z^+, T_P increases with an increase in Z. This is attributed to an enhanced velocity gradient with an increase in Z. To be explicit, the coarser particles are to increase the TKE production rate. On the other hand, the $E_D(z^+)$ profiles for different Z (= 2, 1, 0.5 and 0.25) are shown in figure 11. As the $E_D \sim k^{3/2}$, an enlarged frame bounded by $z^+ \in [0.9, 1]$ and $E_D \in [0.45, 0.75]$ indicates that for a given z^+, E_D increases with a decrease in Z, indicating that the resulting TKE dissipation rate reduces when coarser particles are mostly present in the two-phase flow system. Figures 10 and 11 show that for a given z^+, the behaviour of $T_P(Z)$ is contrary to that of $E_D(Z)$. This is primarily attributed to the fact that at any vertical distance,

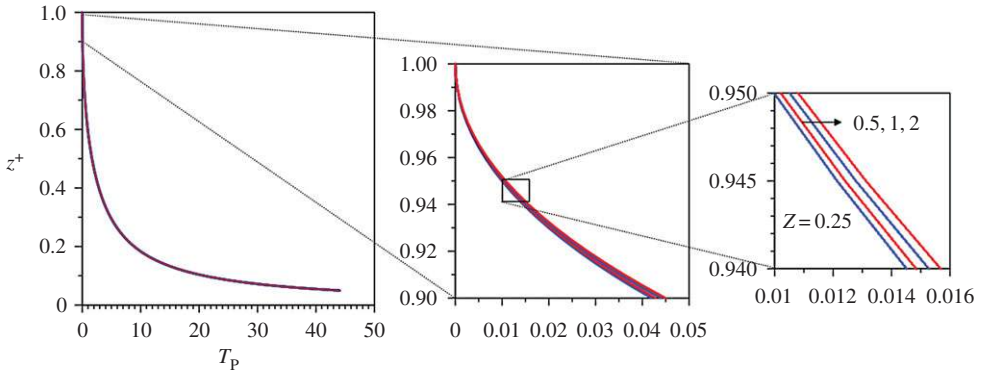

Figure 10. Computed $T_P(z^+)$ profiles for different Z (=0.25, 0.5, 1 and 2). (Online version in colour.)

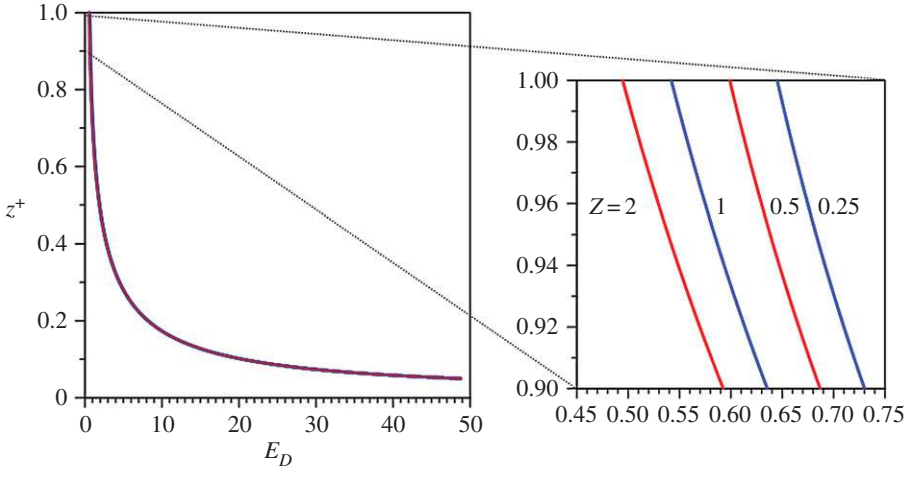

Figure 11. Computed $E_D(z^+)$ profiles for different Z (=2, 1, 0.5 and 0.25). (Online version in colour.)

the TKE diffusion rate, the TKE production rate and the TKE dissipation rate always maintain a dynamic equilibrium from the perspective of the energetics of the two-phase flow system, given by equation (2.29).

To determine the influence of suspended particles on the flow dynamics, the Kolmogorov number (Ko) is often used. For stratified fluids, the Kolmogorov number is similar to the Richardson number. The Ko represents the relative expenditure of TKE production rate to retain the particles in suspension [24]. The Ko is expressed as

$$\mathrm{Ko} = \frac{\Delta g \overline{c'w'}}{\tau(\mathrm{d}\bar{u}/\mathrm{d}z)} = \frac{\kappa^2 \gamma z^+ k^{+1/2}}{(1-z^+)^2} \cdot \frac{Z}{G}\bar{c}(1-\bar{c})^{1+n}. \tag{4.1}$$

Figure 12 depicts the Ko(z^+) profiles for different Z (= 2, 1, 0.5 and 0.25). In general, for a given Z, the Ko slowly increases with z^+ and then its evolution suddenly escalates for a larger z^+. Equation (4.1) reveals that the Ko is affected by k^+, Z and $\bar{c}$. Therefore, in the limit $z^+ \to a^+$, the enlarged frame, bounded by $z^+ \in [0.05, 0.07]$ and $\mathrm{Ko} \in [0, 0.02]$, depicts that for a given z^+, Ko increases with an increase in Z, because the Ko approximately scaled as $\mathrm{Ko} \sim Z$ in the limit $z^+ \to a^+$. It suggests that in the limit $z^+ \to a^+$, the relative expenditure of TKE production rate to retain the

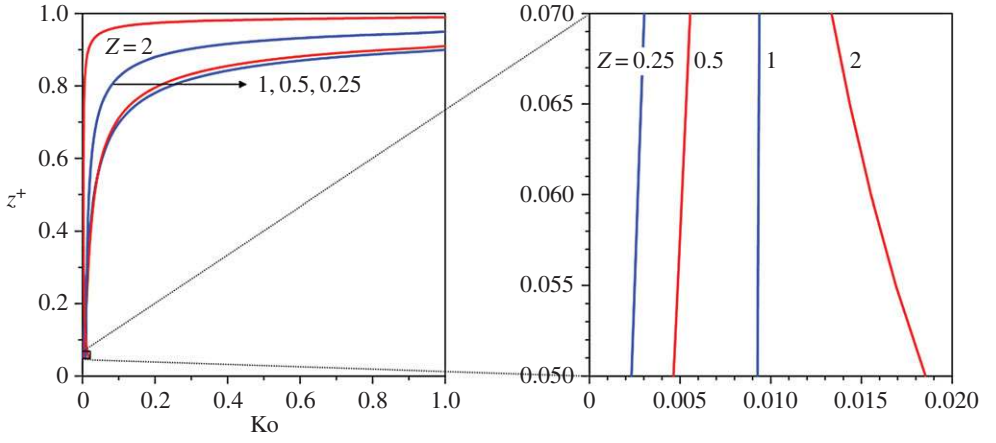

Figure 12. Computed Ko(z^+) profiles for different Z (=2, 1, 0.5 and 0.25). (Online version in colour.)

particles in suspension is more for the coarser particles because the downward settling flux is larger for coarser particles. However, as z^+ increases, the k^+ and $\bar{c}$ diminish at a much faster rate with Z (figures 3 and 6). Therefore, away from the reference level, Ko for a given z^+ increases with a decrease in Z.

Finally, we are interested to explore the behaviour of the inherent turbulent length scales, such as Prandtl's mixing length (l), Taylor microscale (λ) and Kolmogorov length scale (η). In normalized form, they are expressed as

$$l^+ = \left[-\frac{\tilde{\tau}}{(\mathrm{d}u^+/\mathrm{d}z^+)|\mathrm{d}u^+/\mathrm{d}z^+|}\right]^{1/2}, \tag{4.2}$$

$$\lambda^+ = \left(\frac{10k^+}{E_D}\right)^{1/2} J^{-1/2} \tag{4.3}$$

and

$$\eta^+ = E_D^{-1/4} J^{-3/4}, \tag{4.4}$$

where $(l^+, \lambda^+, \eta^+) = (l, \lambda, \eta)/h$, $J = u_* h/\upsilon$ and υ is the coefficient of kinematic viscosity of fluid. Here, we consider $\upsilon = 10^{-6}\ \mathrm{m^2\ s^{-1}}$. Figure 13 depicts the profiles of $l^+(z^+)$, $\lambda^+(z^+)$ and $\eta^+(z^+)$ for different Z in the left panel. On the other hand, the right panel demonstrates the enlarged view of the curves in the small rectangular frames. For a given z^+, l^+ increases with a decrease in Z owing to an increased velocity gradient with an increase in Z. This feature reveals that the effective traversing distance of an eddy from its generation to degeneration reduces with an increase in particle size before transmitting the energy to the ambient fluid. By contrast, λ^+ and η^+ increase with an increase in Z. Equations (4.3) and (4.4) show that the λ^+ is jointly influenced by k^+ and E_D, while the η^+ is solely affected by E_D. Importantly, for a given z^+, both k^+ and E_D increase with a decrease in Z. Therefore, λ^+ is mutually dependent on $k^+(Z)$ and $E_D(Z)$. The enhanced trend of $\eta^+(z^+)$ with an increase in Z corresponds to that of the $E_D(z^+)$ with a decrease in Z. These observations disclose that the characteristic size of an eddy in the inertial subrange and the dissipation range increases with an increase in particle size, as the coarser particles dampen the TKE dissipation rate in the two-phase flow system.

The present mathematical model thus provides a complete picture of the turbulent characteristics of the two-phase flow system by a dynamic coupling of the suspended particle concentration, flow velocity and the energetics of the two-phase flow system. This study, therefore, remedies the existing shortcomings of the diffusion theory by considering the dynamics

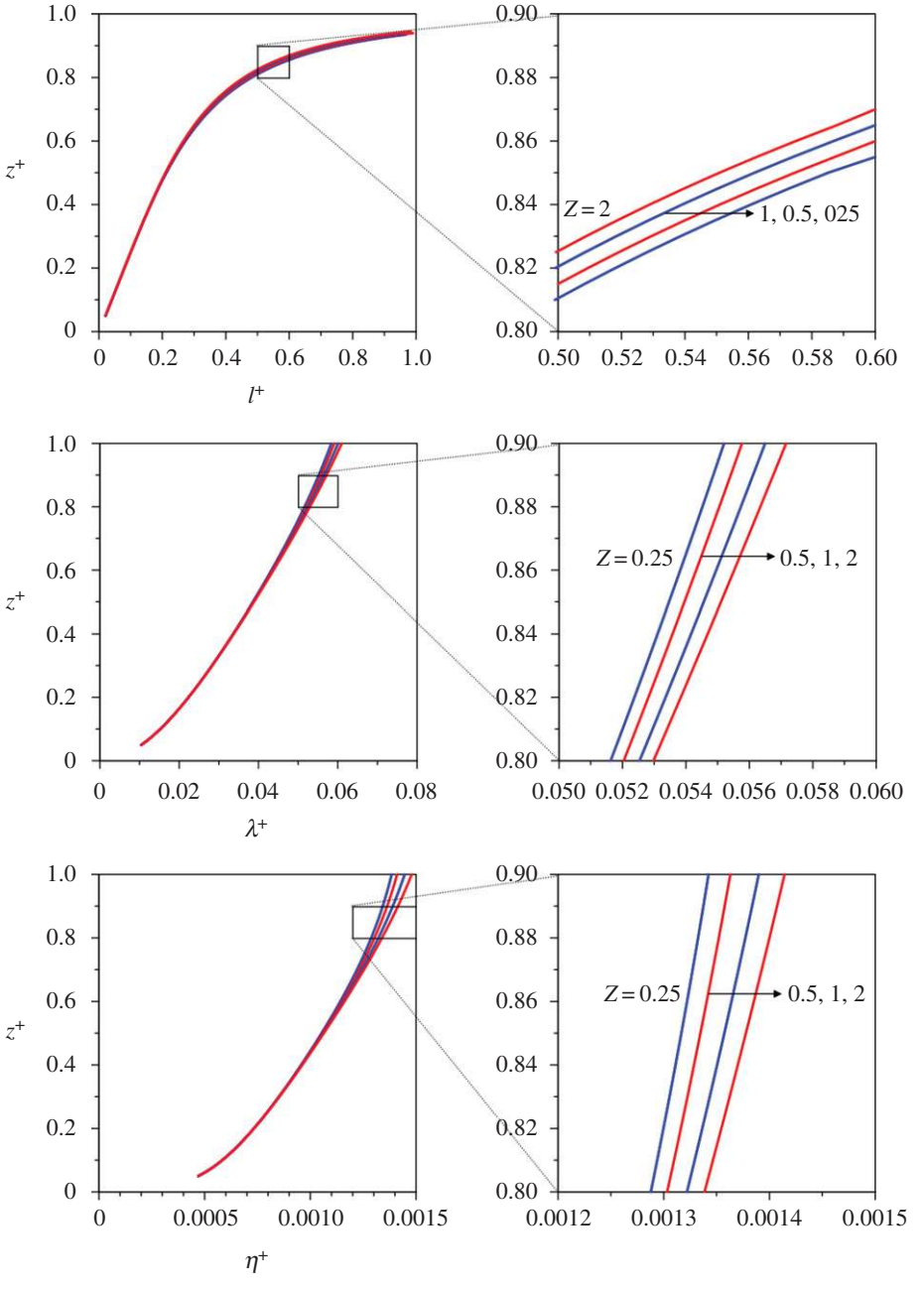

Figure 13. Computed $l(z^+)$, $\lambda(z^+)$ and $\eta(z^+)$ profiles for different Z (=2, 1, 0.5 and 0.25). (Online version in colour.)

of fluid flow that is affected by the presence of suspended solid particles. Moreover, it takes into account the reduction in pulsation energy resulting from the work done to keep the particles in suspension. It can be applied to simulate the advection of suspended particles in loose boundary streams, especially in field conditions. The variations of several key turbulence parameters with the Rouse number demonstrate a clear understanding of the dynamics of the two-phase flow system. However, for the simulation of the dynamics of the two-phase flow system considering the impact of cohesive force and particle collisions, further investigation is required as a future scope of research.

5. Conclusion

A mathematical model of the two-phase flow system is developed by a dynamic coupling of the suspended particle concentration, flow velocity and the energetics of the two-phase flow system. The main conclusions of the study are as follows:

(i) The Reynolds shear stress in a two-phase flow system still obeys a linear law when the fluid velocity fluctuations are replaced by the velocity fluctuations of the two-phase flow system.

(ii) Unlike the suspended particle concentration profile obtained from the Rouse equation, the concentration profiles obtained from this study do not vanish at the free surface. However, the concentration reduces with an increase in the Rouse number. On the other hand, the horizontal velocity component marginally increases with an increase in the Rouse number owing to an enhanced velocity gradient, while the TKE decreases.

(iii) The TKE flux, diffusion and production rates increase with an increase in the Rouse number. On the contrary, the TKE dissipation rate increases with a decrease in the Rouse number.

(iv) In close proximity of the reference level, the Kolmogorov number increases with an increase in the Rouse number. However, away from the reference level, it increases with a decrease in the Rouse number.

(v) The Prandtl's mixing length increases with a decrease in the Rouse number. It results from an increased velocity gradient with an increase in the Rouse number. By contrast, the Taylor microscale and the Kolmogorov length scale increase with an increase in the Rouse number owing to the damping of the TKE dissipation rate by the coarser suspended particles.

Data accessibility. The theoretical curves of this study were obtained from the solutions of the equations developed in this paper. The references of the experimental data of various authors are furnished in the figures. All the data of this study can be obtained from the authors.

Authors' contributions. The authors of this paper contributed jointly.

Competing interests. The authors declare that they have no competing interests.

Funding. The study is not funded by any agency.

References

1. Taylor GI. 1921 Diffusion by continuous movements. *Proc. Lond. Math. Soc.* **20**, 196–212. (doi:10.1112/plms/s2-20.1.196)
2. Rouse H. 1937 Modern conceptions of the mechanics of fluid turbulence. *Trans. Am. Soc. Civ. Eng.* **102**, 463–505.
3. Dey S. 2014 *Fluvial hydrodynamics: hydrodynamic and sediment transport phenomena*. Berlin, Germany: Springer.
4. Hunt JN. 1954 The turbulent transport of suspended sediment in open channels. *Proc. R. Soc. Lond. A* **224**, 322–335. (doi:10.1098/rspa.1954.0161)
5. Velikanov MA. 1954 Principle of the gravitational theory of the movement of sediments. *Acad. Sci. Bull. Geophys. Ser* **4**, 349–359.
6. Velikanov MA. 1958 *Alluvial process (fundamental principles)*. State Publishing House of Theoretical and Technical Literature, Russia.
7. Montes JS. 1973 Interaction of two dimensional turbulent flow with suspended particles. PhD thesis, Massachusetts Institute of Technology, Cambridge, MA, USA.
8. Coleman NL. 1986 Effects of suspended sediment on the open-channel velocity distribution. *Water Resour. Res.* **22**, 1377–1384. (doi:10.1029/WR022i010p01377)
9. Lyn DA. 1986 Turbulence and turbulent transport in sediment-laden open-channel flows. PhD thesis, California Institute of Technology, Pasadena, CA, USA.
10. Guo JK, Julien PY. 2001 Turbulent velocity profiles in sediment laden flows. *J. Hydraul. Res.* **39**, 11–23. (doi:10.1080/00221680109499798)

11. Cellino M, Graf WH. 1999 Sediment-laden flow in open-channels under noncapacity and capacity conditions. *J. Hydraul. Eng.* **125**, 455–462. (doi:10.1061/(ASCE)0733-9429(1999)125:5(455))
12. Nikora VI, Goring DG. 2002 Fluctuations of suspended sediment concentration and turbulent sediment fluxes in an open-channel flow. *J. Hydraul. Eng.* **128**, 214–224. (doi:10.1061/(ASCE)0733-9429(2002)128:2(214))
13. Bennett SJ, Hou Y, Atkinson JF. 2014 Turbulence suppression by suspended sediment within a geophysical flow. *Environ. Fluid Mech.* **14**, 771–794. (doi:10.1007/s10652-013-9323-2)
14. Pedinotti S, Mariotti G, Banerjee S. 1992 Direct numerical simulation of particle behaviour in the wall region of turbulent flows in horizontal channels. *Int. J. Multiph. Flow* **18**, 927–941. (doi:10.1016/0301-9322(92)90068-R)
15. Elghobashi S, Truesdell GC. 1993 On the two-way interaction between homogeneous turbulence and dispersed solid particles. I: Turbulence modification. *Phys. Fluids A* **5**, 1790–1801. (doi:10.1063/1.858854)
16. Yang CY, Lei U. 1998 The role of the turbulent scales in the settling velocity of heavy particles in homogeneous isotropic turbulence. *J. Fluid Mech.* **371**, 179–205. (doi:10.1017/S0022112098002328)
17. Hsu TJ, Jenkins JT, Liu PLF. 2003 On two-phase sediment transport: dilute flow. *J. Geophys. Res.* **108**, 1–14. (doi:10.1029/2001JC001276)
18. Nielsen P, Teakle IAL. 2004 Turbulent diffusion of momentum and suspended particles: a finite-mixing-length theory. *Phys. Fluids* **16**, 2342–2348. (doi:10.1063/1.1738413)
19. Chou YJ, Fringer OB. 2008 Modeling dilute sediment suspension using large-eddy simulation with a dynamic mixed model. *Phys. Fluids* **20**, p115103, 1–13. (doi:10.1063/1.3005863)
20. Hsu TJ, Jenkins JT, Liu PLF. 2004 On two-phase sediment transport: sheet flow of massive particles. *Proc. R. Soc. Lond. A* **460**, 2223–2250. (doi:10.1098/rspa.2003.1273)
21. Mueller S, Llewellin EW, Mader HM. 2010 The rheology of suspensions of solid particles. *Proc. R. Soc. A* **466**, 1201–1228. (doi:10.1098/rspa.2009.0445)
22. Cantero-Chinchilla FN, Castro-Orgaz O, Dey S. 2016 Distribution of suspended sediment concentration in wide sediment-laden streams: a novel power-law theory. *Sedimentology* **63**, 1620–1633. (doi:10.1111/sed.12276)
23. Barenblatt GI. 1953 On the motion of suspended particles in a turbulent flow. *Prikladnaya Matematika i Mekhanika* (*Applied Mathematics and Mechanics* (*PMM*)) **17**, 261–274.
24. Barenblatt GI. 1996 *Scaling, self-similarity, and intermediate asymptotics*. Cambridge, UK: Cambridge University Press.
25. Monin AS, Yaglom AM. 1971 *Statistical fluid mechanics: mechanics of turbulence*, vol. 1. Boston, MA: MIT Press.
26. Richardson JF, Zaki WN. 1954 Sedimentation and fluidisation, part I. *Trans. IChE* 32, 35–53.